applied sciences

MDPI

Article

The Suppression Characteristics of $NH_4H_2PO_4$/Red Mud Composite Powders on Methane Explosion

Yimin Zhang [1,2], Yan Wang [1,2,*], Xiangqing Meng [1,2], Ligang Zheng [1,2] and Jianliang Gao [1,2,*]

1 The Collaboration Innovation Center of Coal Safety Production of Henan Province, Henan Polytechnic University, Jiaozuo 454000, Henan, China; knmglss@sina.com (Y.Z.); mxq0508123@126.com (X.M.); zhengligang97@163.com (L.Z.)

2 State Key Laboratory Cultivation Bases Gas Geology and Gas Control, College of Safety Science and Engineering, Henan Polytechnic University, Jiaozuo 454000, Henan, China

* Correspondence: yanwang@hpu.edu.cn (Y.W.); gao@hpu.edu.cn (J.G.); Tel.: +86-391-398-7440 (Y.W. & J.G.)

Received: 15 July 2018; Accepted: 20 August 2018; Published: 22 August 2018

Abstract: The composite powders composed of red mud (RM) and $NH_4H_2PO_4$ ($NH_4H_2PO_4$/RM) were successfully prepared by the anti-solvent method. The composition and structure of the $NH_4H_2PO_4$/RM composite powders were characterized by the techniques of X-ray diffraction (XRD), SEM, N_2 adsorption-desorption and Thermogravimetry-Differential scanning calorimetry (TG-DSC). The analysis results indicate that the as-prepared samples are composed with uniform nanoparticles and possess the porous structure. The methane explosion suppression characteristics of the $NH_4H_2PO_4$/RM composite powders were tested by a 20 L spherical explosion system and a 5 L pipe test system. The results show that the $NH_4H_2PO_4$/RM composite powders possess considerable suppression properties on methane explosion. When the loading content of $NH_4H_2PO_4$ reached 30%, the maximum pressure and the maximum pressure rise rate of methane explosion were decreased by 35.1% and 95.8%, respectively. When comparing with no powder addition, the time to reach the pressure peak was extended from 0.07 s to 0.50 s. The $NH_4H_2PO_4$/RM composite powders presented a synergistic suppression effect between $NH_4H_2PO_4$ and RM, which made it exhibit considerable suppression property than that of pure $NH_4H_2PO_4$ or red mud powders.

Keywords: $NH_4H_2PO_4$/RM composite powders; methane explosion; suppression characteristics; synergistic suppression effect

1. Introduction

Gas explosion is an extraordinary serious coal mine disaster that can cause massive damage and casualties. In order to reduce the impact of coal mine gas explosion, researchers have carried out a lot of research works. On the one hand, the refuge chamber has been widely investigated and used for miners who are unable to escape during an accident, which can provide basic survival conditions [1–3]. Zhao et al. simulated and analyzed the structure strength of a coal mine mobile refuge chamber under gas explosion load by a finite element method [4]. Li et al. simulated and analyzed the air pressure distribution law in the mine refuge chamber [5]. Zhang et al. studied the design and optimation of the refuge chambers based on the simulation of the gas explosion pressure fields [6]. Jia et al. studied the relationship between the propagation regulation about shock wave of gas explosion and the laneway cross-sectional area [7]. Zhang et al. established the underground mine tunnel model and the refuge chamber model by using the finite element software ANSYS/LA-DYNA, the propagation of methane/air mixture blast waves, and the fluid-structure interactions were also simulated by the Arbitrary Lagrange-Euler (ALE) method [8].

On the other hand, the suppression of gas explosion in the coal mine is also significant for the safety of mine production. Methane is the major component of mine gas and its explosion limits is 5–15%. In the previous studies, water mists [9–12], inert gas [13–16], and chemical powders [17–21] have been used to suppress the methane explosion. Because of its excellent performance on methane explosion suppression, chemical powders are studied extensively. In recent years, the composite powders were appreciated and studied widely for its synergistic effect on the explosion suppression. Harris et al. systematically studied the relationship between the particle size distributions, specific surface area, and the explosion suppression effectiveness of the rock dusts [22]. Ni et al. fabricated a new type fire suppressant with core–shell structure while using zeolites and $NaHCO_3$ [23]. The composites could extinguish the oil fire with less powder amount and shorter time when comparing with the common BC (. . .) powders. Bertolino et al. report a novel procedure to fabricate multilayer composite biofilms based on halloysite nanotubes (HNTs) and sustainable polymers [24]. The thermal properties analysis of the nanocomposite indicated that the chitosan/halloysite layer generates a flame retardant action on the biomaterials and the multilayer morphology confers a fire resistance to the nanocomposite. In our previous work, the $NaHCO_3$/red-mud composite powders were prepared and its suppression effect on the methane explosion was tested in detail [25]. Due to the synergistic suppression effect between $NaHCO_3$ and red-mud, the $NaHCO_3$/red-mud composite powders exhibited better suppression properties than that of the pure $NaHCO_3$ and red mud powders. Thus, the use of composite powders gradually became an important development trend for the gas explosion suppression.

Red mud is the waste residue of alumina industry, which is mainly composed of Al_2O_3, CaO, SiO_2, and Fe_2O_3, and caused serious environmental pollution. The recycle and utilization of red mud have become an urgent problem. On this condition, many works have been done to find the novel utilization of red mud [26–30]. In our previous research, the red mud was modified by a facile method and presented a considerable suppression property on methane explosion [31]. Producing methane explosion suppression reagents with red mud could both solve the pollution problem and bring considerable economic value. $NH_4H_2PO_4$ is a kind of common fire-extinguishing agent. Kordylewski and Amrogowicz studied the suppression effect of $NH_4H_2PO_4$ and $NaHCO_3$ powders on the methane explosion, and the results indicated that the $NH_4H_2PO_4$ powders had a better suppression effect on the methane explosion [32]. However, to the best of our knowledge, there is still no research about the preparation and methane explosion suppression application of the $NH_4H_2PO_4$ and red mud composite powders.

Herein, a new composite ($NH_4H_2PO_4$/RM) for methane explosion suppression was successfully prepared with $NH_4H_2PO_4$ and red mud. The composition and structure of the $NH_4H_2PO_4$/RM composite powders were characterized, and their methane explosion suppression properties were tested in detail. Furthermore, the suppression mechanism of the $NH_4H_2PO_4$/RM composite powders on methane explosion was also discussed.

2. Materials and Methods

2.1. Materials

$NH_4H_2PO_4$/RM composite powders were prepared with the modified red mud and $NH_4H_2PO_4$ particles by an anti-solvent method. The raw red mud was provided by Henan Zhongmei Aluminum Corporation, China (major compositions: SiO_2 16.94 wt %; Al_2O_3 23.25 wt %; Fe_2O_3 15.05 wt %; CaO 16.94 wt %; TiO_2 4.27 wt %; Na_2O 3.72 wt %; MgO 1.93 wt %). The raw red mud was dried, ground, and sieved to a size of <150 μm. Other chemical reagents were of analytical grade. The modified red mud powders were prepared at first and the method was shown in the literature [31]. The preparation process of $NH_4H_2PO_4$/RM composite powders with different weight percentage of $NH_4H_2PO_4$ (5%, 10%, 15%, 10%, 25%, and 30%) was as follows. Firstly, a certain amount of $NH_4H_2PO_4$ was solved in deionized water to become a saturated solution. Then, 10 g modified red mud powders were dispersed in the anti-solvent ethanol to become a suspension solution. Under magnetic stirring, the prepared suspension solution of modified red mud was

added into the $NH_4H_2PO_4$ saturated solution. The obtained mixture was stirred for 2 h, aged for 4 h, and then the precipitate was separated by filtration and dried in vacuum for 12 h. Finally, $NH_4H_2PO_4$/RM composite powders with a different weight percentage of $NH_4H_2PO_4$ were obtained, and denoted as 5%-$NH_4H_2PO_4$/RM, 10%-$NH_4H_2PO_4$/RM, 15%-$NH_4H_2PO_4$/RM, 20%-$NH_4H_2PO_4$/RM, 25%-$NH_4H_2PO_4$/RM, and 30%-$NH_4H_2PO_4$/RM.

2.2. Characterization

X-ray diffraction (XRD) analysis was carried on Bruker-AXS D8 (Bruker, Madison, WI, USA) with CuKα radiation at 40 kV and 25 mA. Field emission scanning electron microscopy (FESEM, Quanta™ 250 FEG) (FEI, Eindhoven, The Netherlands) was used to analyze the morphologies of the prepared samples. N_2 adsorption-desorption isotherms were obtained on a Quantachrome Autosorb-iQ sorption analyzer (Quantachrome, Boynton Beach, FL, USA). Before carrying out the measurement, the samples were degassed at 150 °C for more than 6 h. The specific surface areas (S_{BET}) of the samples were calculated while following the multi-point BET (Brunauer-Emmett-Teller) procedure. Thermogravimetry-Differential scanning calorimetry (TG-DSC) analysis was completed on a Simultaneous Thermal Analyzer (NETZSCH, Selb, Germany) in a flow of air (20 mL·min^{-1}) at a heating rate of 10 °C·min^{-1}.

2.3. Explosion Experiment Device and Test Process

The effects on the methane-air premixed gas explosion pressure of $NH_4H_2PO_4$/RM composite powders with different weight percentage of $NH_4H_2PO_4$ were tested by the 20 L spherical explosion system. The illustration of 20 L spherical explosion system was presented in Figure 1. The system mainly includes the gas distribution system, ignition system, powder injection system, and data acquisition system. Firstly, the 9.5% methane/air was mixed by the partial pressure method. Then, the $NH_4H_2PO_4$/RM composite powders were put into the powder storage tank and the 2 MPa injection air was introduced into the tank. The high-pressure air and the powders were injected and dispersed into the spherical vessel after pushing the ignition button. The igniter is electrical pulse and the ignition energy is about 100 J. The explosion pressure was collected by the pressure sensor and then saved by the computer at the same time.

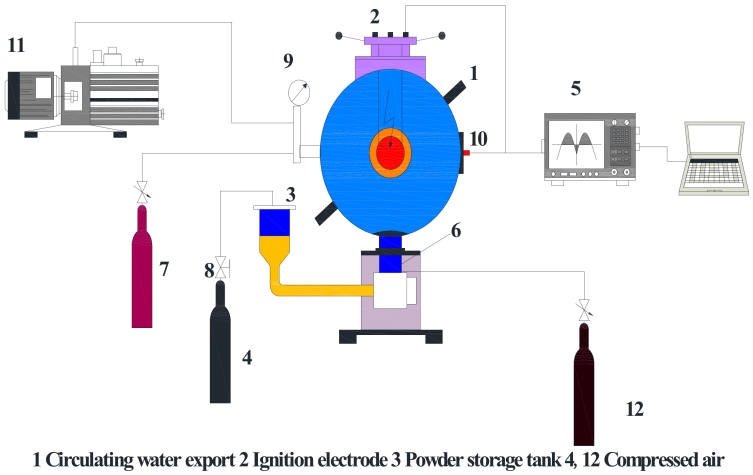

Figure 1. The illustration of 20 L spherical explosion system.

The average velocity of flame propagation was measured by a pipe test system with a cross-sectional area of 100 × 100 mm^2 and a length of 500 mm. The illustration of the pipe test system was shown in our previous published paper [18]. Firstly, the $NH_4H_2PO_4$/RM composite powders

were put into the powder container. Then, the premixed 9.5% methane/air was introduced into the pipe. The powders were injected into the pipe by the high-pressure gas and then the methane/air was ignited by the electrical pulse igniter. Meanwhile, the flame propagation images were captured by a high-speed camera and saved in the computer.

3. Results and Discussion

3.1. Sample Characterization

The X-diffraction patterns of $NH_4H_2PO_4$/RM composite powders, red mud, and $NH_4H_2PO_4$ are shown in Figure 2, respectively. From Figure 2, we can see that the $NH_4H_2PO_4$/RM composite powders and red mud powders have the similar X-ray diffraction patterns. The diffraction patterns of the composite powders also present the characteristic diffraction peaks of $NH_4H_2PO_4$ (2θ = 19.6°, 27.6°, 36.4°, 42.1°) after loading the $NH_4H_2PO_4$ particles. The results indicate that the red mud was the main component of the composite powders and the $NH_4H_2PO_4$ particles were loaded on the red mud successfully.

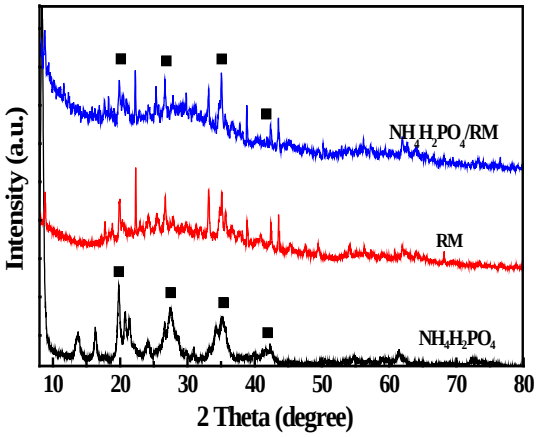

Figure 2. X-ray diffraction (XRD) patterns of $NH_4H_2PO_4$/RM composite powders, red mud (RM), and $NH_4H_2PO_4$.

The SEM images of $NH_4H_2PO_4$ powders, red mud, and the $NH_4H_2PO_4$/RM composite powders are shown in Figure 3. As shown in Figure 3A, the sizes of $NH_4H_2PO_4$ particles are large and not uniform, and the diameters are from 5 to 20 μm. The surface of red mud is rich in pores and the pores are in irregular distribution, as shown in Figure 3B. The surface of the $NH_4H_2PO_4$/RM is coated with small particles according to Figure 3C, which indicates that $NH_4H_2PO_4$ are successfully loaded on the surface of red mud, forming the uniform composite powders.

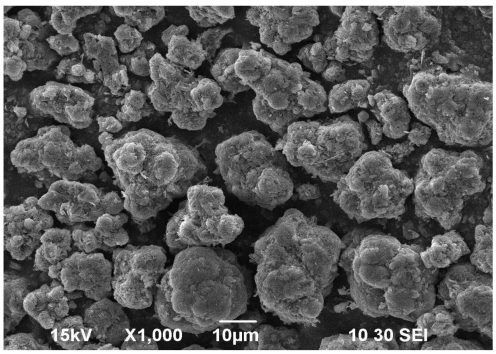

(**A**)

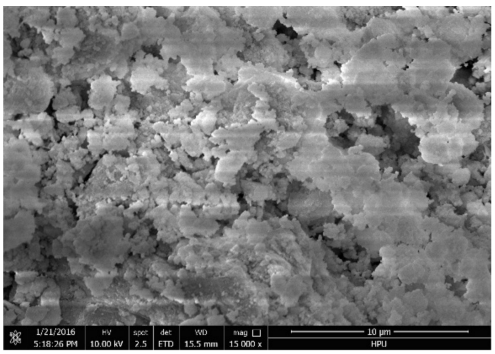

(**B**)

Figure 3. *Cont.*

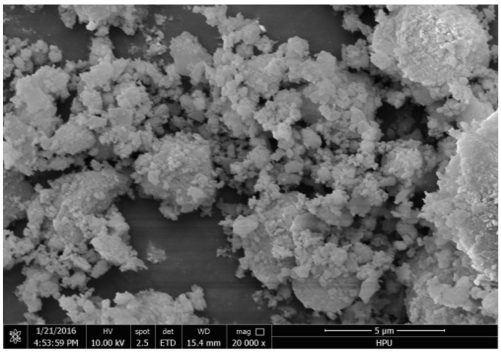

(**C**)

Figure 3. SEM images of $NH_4H_2PO_4$ particles (**A**), red mud (**B**), and the $NH_4H_2PO_4$/RM composite powders (**C**).

The N_2 adsorption-desorption isotherms of red mud and the $NH_4H_2PO_4$/RM composite powders are shown in Figure 4. Both of the isotherms are type IV in the IUPAC classification with the H4 hysteresis loop. The results indicate that these two powders possess the mesoporous structure, and capillary condensation occurred during the adsorption-desorption process. After loading the $NH_4H_2PO_4$ particles, the adsorption capacity of the composite is lower than red mud in the P/P_0 range of 0.5–1.0, indicating the decrease of mesopores in the $NH_4H_2PO_4$/RM composite powders and the formation of a granulation structure during the loading process. The data of this experiment confirmed the changes of the $NH_4H_2PO_4$/RM morphology that are presented in SEM images (Figure 3). The specific surface area and pore volume of red mud are 123.16 $m^2 \cdot g^{-1}$ and 0.158 $cm^3 \cdot g^{-1}$. After loading the $NH_4H_2PO_4$ particles, the data of the composite powders are reduced to 75.83 $m^2 \cdot g^{-1}$ and 0.116 $cm^3 \cdot g^{-1}$. It means that the $NH_4H_2PO_4$ particles were loaded on the surface and/or in the pore of red mud.

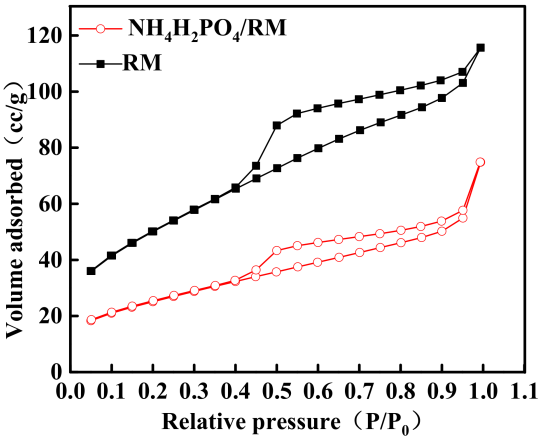

Figure 4. N_2 adsorption-desorption isotherms of $NH_4H_2PO_4$/RM composite powders and RM.

The TG-DSC curves of the $NH_4H_2PO_4$/RM composite powders are shown in Figure 5. From the TG curve, there are three weight loss stages in the whole process. The first stage from 120 °C to 220 °C is attributed to the lost and the thermal decomposition of adsorbed and intercalated moisture of the $NH_4H_2PO_4$/RM composite powders. The second stage from 220 °C to 300 °C could be ascribed to the decomposition of $NH_4H_2PO_4$. The third stage from 300 °C to 420 °C could be ascribed to the decomposition of the hydroxides (such as: $Al(OH)_3$ and $Fe(OH)_3$). After 420 °C, there is no further weight loss, indicating that the composite powder became stable. The total weight loss of the $NH_4H_2PO_4$/RM composite powders is 93.7%. The DSC curve of the composite powders exhibited three endothermic peaks, which is consistent with the TG curve. According to the DSC curve, the total

endothermic quantity of the $NH_4H_2PO_4$/RM composite powders is 1257.9 $J \cdot g^{-1}$, indicating that the composite powders presented an excellent heat absorption performance.

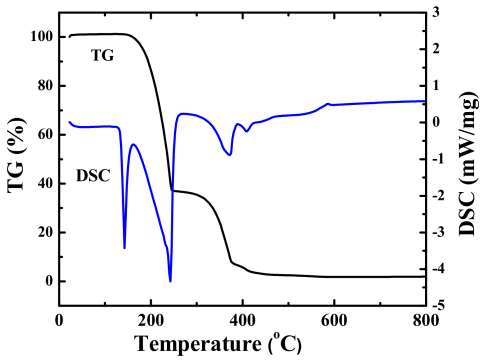

Figure 5. Thermogravimetry-Differential scanning calorimetry (TG-DSC) curves of the $NH_4H_2PO_4$/RM composite powders.

3.2. Suppression Properties of the $NH_4H_2PO_4$/RM Composite Powders

The suppression properties of the $NH_4H_2PO_4$/RM composite powders with different amount of $NH_4H_2PO_4$ (weight percentage of 5%, 10%, 15%, 20%, 25%, and 30%) were tested and the results are presented in Figure 6. Figure 6A shows the 9.5% premixed methane-air explosion pressure curves with no powders, pure red mud powders, and the $NH_4H_2PO_4$/RM composite powders. It can be seen from Figure 6A that the maximum explosion pressure is decreased and the time of pressure peak arriving is delayed by adding suppression powders. The explosion suppression effect of red mud was improved after loading $NH_4H_2PO_4$, and enhanced gradually with increasing the amount of $NH_4H_2PO_4$. When the loading amount is more than 20%, the suppression performance of the $NH_4H_2PO_4$/RM composite powders on the maximum explosion pressure is even better than the pure $NH_4H_2PO_4$ powders. The 30%-$NH_4H_2PO_4$/RM composite powders show a better suppression effect than the pure $NH_4H_2PO_4$ powders both in the maximum explosion pressure and the time of pressure peak arriving. The maximum rate of pressure rise and the time of pressure peak arriving of the $NH_4H_2PO_4$/RM composite powders and the pure $NH_4H_2PO_4$ and red mud (RM) powders are illustrated in Figure 6B, and the detailed data are shown in Table 1.

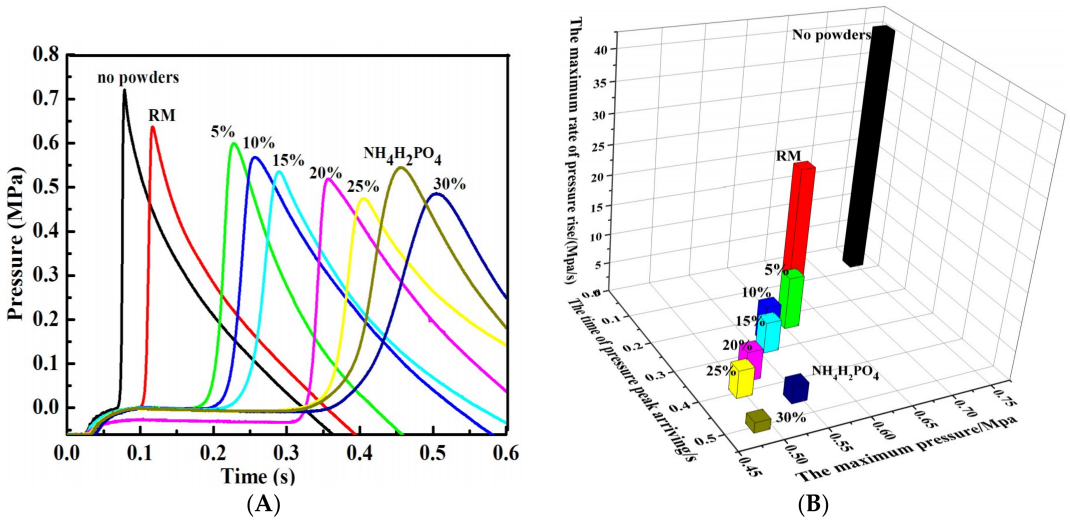

Figure 6. The suppression effect of $NH_4H_2PO_4$/RM composite powders: the explosion pressure curves (**A**), the maximum pressure, the maximum rate of pressure rise, and the time of pressure peak arriving (**B**).

From Table 1, we can see that when adding the 30% $NH_4H_2PO_4$/RM composite powders as the suppression agent, the maximum explosion pressure is decreased from 0.749 MPa (no powders) to 0.486 MPa, which reduce 35.1%. Accordingly, the maximum rate of pressure rise is decreased from 41.16 MPa·s^{-1} to 1.72 MPa·s^{-1}, which reduce 95.8%, and the delay time of pressure peak arriving is increased from 0.07 s to 0.50 s, which delay 0.43 s.

Table 1. The explosion parameters of methane-air premixed gas with different powders.

Samples	Max Pressure (MPa)	The Rate of Max-Pressure Rise (MPa·s^{-1})	Time of Pressure Peak Arriving (s)	Decline Rate of Max Pressure (%)	Decline Rate of Max Pressure Rise (%)	Delay Time of Pressure Peak Arriving (s)
No powders	0.749	41.16	0.07	0	0	0
RM	0.651	21.48	0.11	13.1	47.8	0.04
5%-$NH_4H_2PO_4$/RM	0.607	8.79	0.23	19.9	78.6	0.16
10%-$NH_4H_2PO_4$/RM	0.571	6.16	0.26	23.8	85.1	0.19
15%-$NH_4H_2PO_4$/RM	0.562	5.17	0.29	24.9	87.4	0.22
20%-$NH_4H_2PO_4$/RM	0.519	4.32	0.36	30.7	89.5	0.29
25%-$NH_4H_2PO_4$/RM	0.497	2.54	0.40	33.6	93.8	0.33
30%-$NH_4H_2PO_4$/RM	0.486	1.72	0.50	35.1	95.8	0.43
$NH_4H_2PO_4$	0.545	2.99	0.45	27.2	92.8	0.38

The flame propagation images of the 9.5% premixed methane-air explosion with the red mud, $NH_4H_2PO_4$, and the $NH_4H_2PO_4$/RM composite powders are shown in Figure 7. As shown in this figure, the time of explosion flame propagating to the top of the pipe is 26 ms with no powders addition. When the pure red mud or the $NH_4H_2PO_4$ powders was added, the time is 50 ms and 132 ms, respectively. When the $NH_4H_2PO_4$/RM composite powders with the different amount of $NH_4H_2PO_4$ (5%, 10%, 15%, 20%, 25%, and 30%) were added, the time of explosion flame reached the top are 73 ms, 85 ms, 97 ms, 110 ms, 130 ms, and 160 ms, respectively. The results indicate that the $NH_4H_2PO_4$/RM composite powders present a much better suppression effect on flame propagation speed than that of pure RM powders. In addition, the 30%-$NH_4H_2PO_4$/RM composite powders exhibit the best inhibition performance, which is consistent with the results that were tested by the 20 L spherical explosive system.

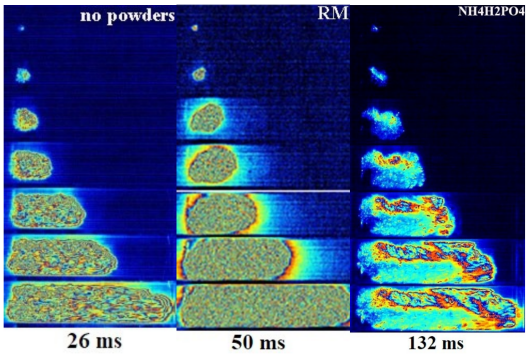

Figure 7. *Cont.*

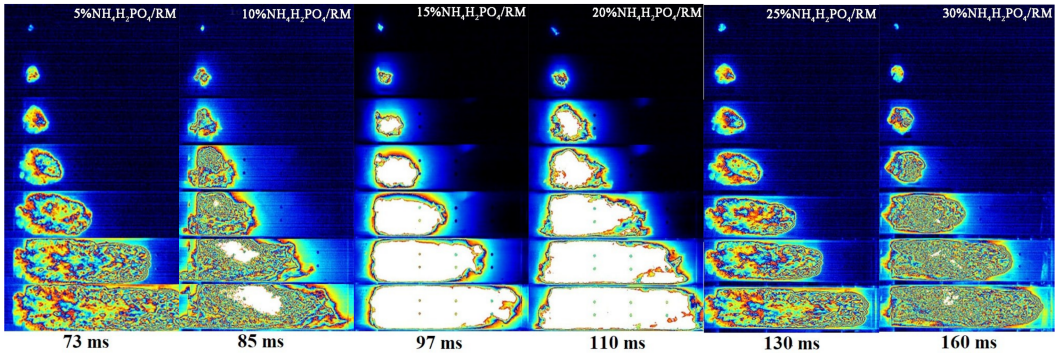

Figure 7. The images of explosion flame in different conditions: no powder, red mud, $NH_4H_2PO_4$ and the $NH_4H_2PO_4$/RM composite powders with different content of $NH_4H_2PO_4$.

3.3. Suppression Mechanism of the $NH_4H_2PO_4$/RM Composite Powders

According to the results of the explosion experiments, the $NH_4H_2PO_4$/RM composite powders present the considerable suppression properties on the methane explosion. The schematic diagram of the $NH_4H_2PO_4$/RM composite powders in the explosion process is illustrated in Figure 8. The suppression mechanism of the $NH_4H_2PO_4$/RM composite powders could be analyzed from two aspects, as follows.

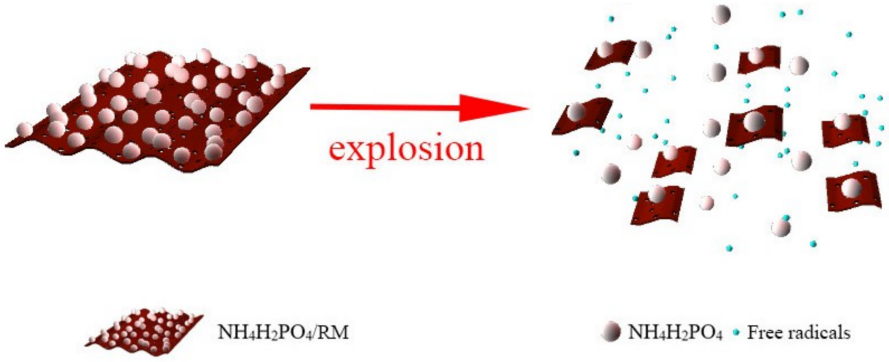

Figure 8. The schematic diagram of the $NH_4H_2PO_4$/RM composite powders in the explosion process.

Physical inhibition effect: The $NH_4H_2PO_4$/RM composite powders have a good heat absorption performance, as shown in the Figure 5. When the composite powders were added into the explosion vessel, the $NH_4H_2PO_4$/RM composite powders were separated into the $NH_4H_2PO_4$ particles and red mud under the high pressure and temperature during the 9.5% premixed methane-air explosion. Then, the $NH_4H_2PO_4$ particles and the hydroxides ($Al(OH)_3$, $Fe(OH)_3$) in the red mud decomposed with absorbing a lot of heat, leading to a good endothermic effect for explosion suppression.

Chemical inhibition effect: The mechanism of methane explosion is shown as the following chain reactions [33].

$$CH_4 + O_2 \rightarrow CH_3 + HO_2$$

$$CH_3 + O_2 \rightarrow CH_2O + HO$$

$$HO + CH_4 \rightarrow CH_3 + H_2O$$

$$CH_2O + HO \rightarrow CH_3 + H_2O$$

$$CH_2O + O_2 \rightarrow HO_2 + CHO$$

$$CHO + O_2 \rightarrow CO + HO_2$$

$$HO_2 + CH_4 \rightarrow H_2O_2 + CH_3$$

$$HO_2 + CH_2O \rightarrow H_2O_2 + CHO$$

During the methane explosion process, the $NH_4H_2PO_4$/RM composite powders decomposed and they generated a lot of gaseous free radicals, which can combine with the generated radicals by methane explosion. In addition, the red mud powders expose more pores on their surface due to the separation of the loaded $NH_4H_2PO_4$ particles, which can adsorb and capture more free radicals that are generated by methane explosion. Both two reasons simultaneously contribute to the chemical inhibition effect of the $NH_4H_2PO_4$/RM composite powders.

4. Conclusions

In this work, the $NH_4H_2PO_4$/RM composite powders with porous structure and high surface area are successfully prepared by using the industrial waste red mud as the base material. The resulting $NH_4H_2PO_4$/RM composite powders are found to possess considerable suppression properties on methane explosion, and the explosion suppression properties enhanced with increasing the amount of $NH_4H_2PO_4$ in the composites. When the loading content of $NH_4H_2PO_4$ reached 30%, the maximum pressure and the maximum pressure rise rate of the 9.5% premixed methane-air explosion were decreased by 35.1% and 95.8%, and the time reached the pressure peak was extended from 0.07 s to 0.50 s. The explosion suppression properties of $NH_4H_2PO_4$/RM composite powders are caused by the physical and chemical inhibition effect. Due to the unique properties and high-value utilization of the waste from the aluminum industry, the $NH_4H_2PO_4$/RM composite powders could be a desirable and economical inhibitor for the methane explosion suppression application.

Author Contributions: Y.Z., X.M. and L.Z. managed all the experimental and performed the experiments and analyzed the data; Y.W. and J.G. conceived and designed the experiments and writing process as the corresponding authors; all authors discussed the results and commented on the manuscript.

Funding: This work was supported by the National Natural Science Foundation of China (51874120, 51504083, 51674104), Program for Science & Technology Innovation Talents in Universities of Henan Province (19HASTIT042), Project funded by China Postdoctoral Science Foundation (2016M592290), the Research Foundation for Youth Scholars of Higher Education of Henan Province (2017GGJS053), the Fundamental Research Funds for the Universities of Henan Province (NSFRF1606), Program for Innovative Research Team in University of Ministry of Education of China (IRT_16R22), Program for Innovative Research Team of Henan Polytechnic University (T2018-2), Foundation for Distinguished Young Scientists of Henan Polytechnic University (J2017-3) and the State Key Laboratory Cultivation Base for Gas Geology and Gas Control (Henan Polytechnic University) (WS2017A03).

Conflicts of Interest: The authors declare no conflict of interest.

References

1. Yang, D.M. The construction and development of the emergency refuge system in coal mine. *J. Saf. Sci. Technol.* **2010**, *11*, 6–9.
2. Mitchell, M.D. Analysis of Underground Coal Mine Refuge Shelters. Ph.D. Thesis, West Virginia University, Morgantown, WV, USA, 20 April 2008.
3. Sun, J.P. The function and configuration scheme in coal mine. *Ind. Mine Autom.* **2010**, *11*, 1–4.
4. Zhao, H.J.; Qian, X.M.; Li, J. Simulation analysis on structure safety of coal mine mobile refuge chamber under explosion load. *Saf. Sci.* **2012**, *50*, 674–678. [CrossRef]
5. Li, F.W.; Jin, L.Z.; Zhan, Z.N. Numerical simulation study of air distribution law of air pressure system in the mine refuge chamber. *J. Theor. Appl. Inf. Technol.* **2012**, *45*, 205–211.
6. Zhang, B.Y.; Zhao, W.; Wang, W.; Zhang, X.H. Pressure characteristics and dynamic respond of coal mine refuge chamber with underground gas explosion. *J. Loss Prev. Process Ind.* **2014**, *30*, 37–46. [CrossRef]
7. Jia, Z.W.; Jing, G.X.; Cheng, L. Study on propagation regulation about shock wave of gas explosion at laneway area break. *China Saf. Sci. J.* **2007**, *17*, 92–94.
8. Zhang, B.Y.; Zhai, D.X.; Wang, W. Failure mode analysis and dynamic response of a coal mine refuge chamber with a gas explosion. *Appl. Sci.* **2016**, *6*, 145. [CrossRef]

9. Yu, M.G.; Wan, S.J.; Xu, Y.L.; Zheng, K.; Liang, D.L. The influence of the charge-to-mass ratio of the charged water mist on a methane explosion. *J. Loss Prev. Process Ind.* **2016**, *41*, 68–76. [CrossRef]
10. Cao, X.Y.; Ren, J.J.; Zhou, Y.H.; Wang, Q.J. Suppression of methane explosion by ultrafine water mist containing sodium chloride additive. *J. Hazard. Mater.* **2015**, *285*, 311–318. [CrossRef] [PubMed]
11. Cao, X.Y.; Ren, J.J.; Bi, M.S.; Zhou, Y.H.; Li, Y.M. Experimental research on the characteristics of methane explosion affected by ultrafine water mist. *J. Hazard. Mater.* **2017**, *324*, 489–497. [CrossRef] [PubMed]
12. Xu, Y.L.; Wang, L.Y.; Yu, M.G.; Wan, S.J. Study on the characteristics of gas explosion affected by induction charged water mist in confined space. *J. Loss Prev. Process Ind.* **2016**, *40*, 227–233. [CrossRef]
13. Mitu, M.; Giurcan, V.; Razus, D.; Oancea, D. Inert gas influence on the laminar burning velocity of methane-air mixtures. *J. Hazard. Mater.* **2017**, *321*, 440–448. [CrossRef] [PubMed]
14. Mitu, M.; Giurcan, V.; Razus, D.; Oancea, D. Influence of inert gas addition on propagation indices of methane–air deflagrations. *Process. Saf. Environ.* **2016**, *102*, 513–522. [CrossRef]
15. Wang, Z.R.; Ni, L.; Liu, X.; Jiang, J.C.; Wang, R. Effects of N_2/CO_2 on explosion characteristics of methane and air mixture. *J. Loss Prev. Process Ind.* **2014**, *31*, 10–15. [CrossRef]
16. Jiang, B.Y.; Liu, Z.G.; Tang, M.Y.; Yang, K.; Lv, P.; Lin, B.Q. Active suppression of premixed methaneair explosion propagation by non-premixed suppressant with nitrogen and ABC powder in a semiconfined duct. *J. Nat. Gas Sci. Eng.* **2016**, *29*, 141–149. [CrossRef]
17. Luo, Z.M.; Wang, T.; Tian, Z.H.; Cheng, F.M.; Deng, J.; Zhang, Y.T. Experimental study on the suppression of gas explosion using the gas-solid suppressant of CO_2/ABC powder. *J. Loss Prev. Process Ind.* **2014**, *30*, 17–23. [CrossRef]
18. Zheng, L.G.; Li, G.; Wang, Y.L.; Zhu, X.C.; Pan, R.K.; Wang, Y. Effect of blockage ratios on the characteristics of methane/air explosion suppressed by BC powder. *J. Hazard. Mater.* **2018**, *355*, 25–33. [CrossRef] [PubMed]
19. Nie, B.S.; Yang, L.L.; Ge, B.Q.; Wang, J.W.; Li, X.C. Chemical kinetic characteristics of methane mixture explosion and its affecting factors. *J. Loss Prev. Process Ind.* **2017**, *49*, 675–682. [CrossRef]
20. Cheng, W.M.; Hu, X.M.; Xie, J.; Zhao, Y.Y. An intelligent gel designed to control the spontaneous combustion of coal: Fire prevention and extinguishing properties. *Fuel* **2017**, *210*, 826–835. [CrossRef]
21. Jiang, H.P.; Bi, M.S.; Gao, W.; Gan, B.; Zhang, D.W.; Zhang, Q. Inhibition of aluminum dust explosion by $NaHCO_3$ with different particle size distributions. *J. Hazard. Mater.* **2018**, *344*, 902–912. [CrossRef] [PubMed]
22. Harris, M.L.; Sapko, M.J.; Zlochower, I.A.; Perera, I.E.; Weiss, E.S. Particle size and surface area effects on explosibility using a 20-L chamber. *J. Loss Prev. Process Ind.* **2015**, *37*, 33–38. [CrossRef] [PubMed]
23. Ni, X.M.; Kuang, K.Q.; Yang, D.L.; Jin, X.; Liao, G.X. A new type of fire suppressant powder of $NaHCO_3$/zeolite nanocomposites with core–shell structure. *Fire Saf. J.* **2009**, *44*, 968–975. [CrossRef]
24. Bertolino, V.; Cavallaro, G.; Milioto, S.; Parisi, F.; Lazzara, G. Thermal Properties of Multilayer Nanocomposites Based on Halloysite Nanotubes and Biopolymers. *J. Compos. Sci.* **2018**, *2*, 41. [CrossRef]
25. Wang, Y.; Cheng, Y.S.; Yu, M.G.; Li, Y.; Cao, J.L.; Zheng, L.G.; Yi, H.W. Methane explosion suppression characteristics based on the $NaHCO_3$/red-mud composite powders with core-shell structure. *J. Hazard. Mater.* **2017**, *335*, 84–91. [CrossRef] [PubMed]
26. Rachel, A.P.; Sara, J.C.; Graeme, J.M. Value adding red mud waste: Impact of red mud composition upon fluoride removal performance of synthesised akaganeite sorbents. *J. Environ. Chem. Eng.* **2018**, *6*, 2063–2074.
27. Li, Y.C.; Min, X.B.; Ke, Y.; Chai, L.Y.; Shi, M.Q.; Tang, C.J.; Wang, Q.W.; Liang, Y.J.; Lei, J.; Liu, D.G. Utilization of red mud and Pb/Zn smelter waste for the synthesis of a red mud-based cementitious material. *J. Hazard. Mater.* **2018**, *344*, 343–349. [CrossRef] [PubMed]
28. Singh, S.; Aswath, M.U.; Ranganath, R.V. Effect of mechanical activation of red mud on the strength of geopolymer binder. *Constr. Build. Mater.* **2018**, *177*, 91–101. [CrossRef]
29. Toniolo, N.; Rincón, A.; Avadhut, Y.S.; Hartmann, M.; Bernardo, E.; Boccaccini, A.R. Novel geopolymers incorporating red mud and waste glass cullet. *Mater. Lett.* **2018**, *219*, 152–154. [CrossRef]
30. Cao, J.L.; Yan, Z.L.; Deng, Q.F.; Yuan, Z.Y.; Wang, Y.; Sun, G.; Wang, X.D.; Hari, B.; Zhang, Z.Y. Homogeneous precipitation method preparation of modified red mud supported Ni mesoporous catalysts for ammonia decomposition. *Catal. Sci. Technol.* **2014**, *4*, 361–368. [CrossRef]
31. Yu, M.G.; Kong, J.; Wang, Y.; Zheng, K.; Zheng, L.G. Experimental research on gas explosion suppression by modified red mud. *J. China Coal Soc.* **2014**, *39*, 1289–1294.

32. Kordylewski, W.; Amrogowicz, J. Comparison of $NaHCO_3$ and $NH_4H_2PO_4$ Effectiveness as Dust Explosion Suppressants. *Combust. Flame* **1992**, *90*, 344–345. [CrossRef]
33. Frenklach, M.; Wang, H.; Rabinowitz, M.J. Optimization and analysis of large chemical kinetic mechanisms using the solution mapping method-combustion of methane. *Prog. Energy Combust. Sci.* **1992**, *18*, 47–73. [CrossRef]